The International Journal of
Robotics Research

Design of an active one-degree-of-freedom lower-limb exoskeleton with inertia compensation

Gabriel Aguirre-Ollinger, J Edward Colgate, Michael A Peshkin and Ambarish Goswami

Design of an active one-degree-of-freedom lower-limb exoskeleton with inertia compensation

Gabriel Aguirre-Ollinger, J. Edward Colgate, Michael A. Peshkin and Ambarish Goswami

Abstract

Limited research has been done on exoskeletons to enable faster movements of the lower extremities. An exoskeleton's mechanism can actually hinder agility by adding weight, inertia and friction to the legs; compensating inertia through control is particularly difficult due to instability issues. The added inertia will reduce the natural frequency of the legs, probably leading to lower step frequency during walking. We present a control method that produces an approximate compensation of an exoskeleton's inertia. The aim is making the natural frequency of the exoskeleton-assisted leg larger than that of the unaided leg. The method uses admittance control to compensate for the weight and friction of the exoskeleton. Inertia compensation is emulated by adding a feedback loop consisting of low-pass filtered acceleration multiplied by a negative gain. This gain simulates negative inertia in the low-frequency range. We tested the controller on a statically supported, single-degree-of-freedom exoskeleton that assists swing movements of the leg. Subjects performed movement sequences, first unassisted and then using the exoskeleton, in the context of a computer-based task resembling a race. With zero inertia compensation, the steady-state frequency of the leg swing was consistently reduced. Adding inertia compensation enabled subjects to recover their normal frequency of swing.

Keywords

Exoskeleton, rehabilitation robotics, lower-limb assistance, admittance control

1. Nomenclature

1.1. Symbols

- I_h, b_h, k_h = Moment of inertia (kg m^2), damping ((N m s)/rad) and stiffness ((N m)/rad) of the human limb.
- $\bar{I}_e^d, \bar{b}_e^d, \bar{k}_e^d$ = Virtual moment of inertia, damping and stiffness of the exoskeleton's drive mechanism in the controller's admittance model.
- I_m = Moment of inertia of the exoskeleton's servo motor, reflected on the output shaft.
- b_c, k_c = Exoskeleton cable drive's damping and stiffness.
- I_s = Exoskeleton's output drive inertia (moment of inertia of the mechanical components between the cable and the torque sensor).
- $I_{arm}, b_{arm}, k_{arm}$ = Moment of inertia, damping and stiffness of the exoskeleton's arm.
- I_c = Emulated inertia compensator's gain (kg m^2).
- ω_{lo} = Cutoff frequency (rad/s) of the inertia compensator's low-pass filter.
- $\omega_{n,e}$ = Natural frequency of the exoskeleton drive.

- τ_h = Net muscle torque (N m) acting on the human limb's joint.
- τ_m = Torque exerted by the exoskeleton's actuator.
- τ_s = Torque measured by the exoskeleton's torque sensor.
- w_m = Angular velocity (rad/s) of the servo motor reflected on the output shaft.
- w_s = Angular velocity of the exoskeleton's drive output shaft.
- Ω_h = Root mean square angular velocity (rad/s) of swing of the human limb.
- f_c = Frequency of leg swing (Hz).
- A_c = Amplitude of leg swing (rad).
- x_{ref} = Horizontal position (dimensionless) of the target cursor on the graphic user interface.
- x_h = Horizontal position of the subject's cursor on the graphic user interface.

Northwestern University, Evanston, IL, USA

Corresponding author:
Gabriel Aguirre-Ollinger
Northwestern University, 2145 Sheridan Rd, Evanston, IL 60208, USA
Email: GabrielAguirre2008@u.northwestern.edu

1.2. Transfer functions

- $\mathbf{Y}_e(s)$ = Two-port admittance of the physical exoskeleton's drive.
- $\bar{Y}_e^d(s)$ = Virtual admittance model followed by the admittance controller. It represents the desired admittance of the torque sensor port.
- $Y_e^s(s)$ = Actual closed-loop admittance at the torque sensor port.
- $Y_e^p(s)$ = Closed-loop admittance at the exoskeleton's port of interaction with the user (ankle brace).
- $Y_e^h(s)$ = Admittance of the human leg when coupled to the exoskeleton (defined as the ratio of $w_s(s)$ to $\tau_h(s)$).
- $Z_{\mathrm{arm}}(s)$ = Impedance of the exoskeleton's arm.
- $Z_h(s)$ = Impedance of the human limb.

2. Introduction

In recent years, different types of exoskeletons and orthotic devices have been developed to assist lower-limb motion. Applications for these devices usually fall into either of two broad categories: (1) augmenting the muscular force of healthy subjects, and (2) rehabilitation of people with motion impairments. Most of the existing implementations in the former group are designed to either enhance the user's capability to carry heavy loads (Lee and Sankai, 2003; Kawamoto and Sankai, 2005; Kazerooni et al., 2005; Walsh et al., 2006) or reduce muscle activation during walking (Banala et al., 2006; Lee and Sankai, 2002; Sawicki and Ferris, 2009). Rehabilitation-oriented applications include training devices for gait correction (Banala et al., 2009; Jezernik et al., 2004) and devices that apply controlled forces to the extremities in substitution of a therapist (Veneman et al., 2007).

Although significant advances have been made in the engineering aspects of exoskeleton design (mechatronics, computer control, actuators), the physiological aspects of wearing an exoskeleton are less well understood. A common observation in recent reviews on exoskeleton research (Dollar and Herr, 2008; Ferris et al., 2005, 2007) has been the absence of reports of exoskeletons reducing the metabolic cost of walking. Another little-researched topic has been the effect of an exoskeleton on the agility of the user's movements. At this point we are not aware of any studies addressing how an exoskeleton can affect the user's selected speed of walking, or the ability to accelerate the legs when quick movements are needed.

The present study constitutes a first step towards enabling an exoskeleton to increase the agility of the lower extremities. At preferred walking speeds, the swing leg behaves as a pendulum oscillating close to its natural frequency (Kuo, 2001). The swing phase of walking takes advantage of this pendular motion in order to reduce the metabolic cost of walking. Thus we theorize that a wearable exoskeleton could be used to increase the natural frequency of the legs, and in doing so enable users to walk comfortably at higher speeds. Although a few studies have been conducted

on the modulation of leg swing frequency by means of an exoskeleton (Lee and Sankai, 2005; Uemura et al., 2006), to the best of our knowledge this effect has not yet been linked experimentally to the kinematics and energetics of walking.

The main difficulty in using an exoskeleton to increase the agility of leg movements is that the exoskeleton's mechanism adds extra impedance to the legs. Therefore the mechanism by itself can be expected to make the legs' movements slower, not faster. And while it is quite feasible to mask the weight and the friction of the mechanism using control, compensating for the mechanism's inertia is considerably more difficult due to stability issues (Buerger and Hogan, 2007; Newman, 1992). All other things being equal, the inertia added by the exoskeleton will probably reduce the pendulum frequency of the legs, which can have important consequences on the metabolic cost and the speed of walking. A study by Browning et al. (2007) found that adding masses to the leg increases the metabolic cost of walking. This cost was strongly correlated to the moment of inertia of the loaded leg. A similar study by Royer and Martin (2005) showed that loading the legs increases the swing time and the stride time during walking. The findings from both studies may be explained by the metabolic cost of swinging the leg. In an experiment reported by Doke et al. (2005), subjects swung one leg freely at different frequencies with fixed amplitude. It was found that the metabolic cost of swinging the leg has a minimum near the natural frequency of the leg, and increases with the fourth power of frequency. Thus if the exoskeleton's inertia reduces the natural frequency of the leg it is very likely that users will reduce their chosen frequency of leg swing accordingly.

The notion of compensating for the inertia of the exoskeleton through control leads to an interesting prospect: to not only compensate for the drop in the natural frequency of the legs caused by the exoskeleton's mechanism, but to actually make the natural frequency of the exoskeleton-assisted leg *higher* than that of the unaided leg. This in turn raises two possible research questions. First, if the exoskeleton modifies the natural frequency of the leg, will people modify their frequency of leg swing accordingly? Second, how does the behavior of metabolic cost change when the natural frequency is modified, i.e. does the new natural frequency accurately predict the minimum metabolic cost?

In this paper we address the first question. We present a control method that produces an approximate compensation of an exoskeleton's inertia. We tested our method on a statically mounted, single-degree-of-freedom (DOF) exoskeleton (Aguirre-Ollinger et al., 2007a,b) that assists the user in performing knee flexions and extensions. The exoskeleton has a 'baseline' mode of operation in which an admittance controller masks the weight and the dissipative effects (friction, damping) of the exoskeleton's mechanism, thereby making the exoskeleton behave as a pure inertia. An acceleration feedback loop is then added to compensate for the exoskeleton's inertia at low frequencies. We conducted an experiment in which subjects performed a multiple series
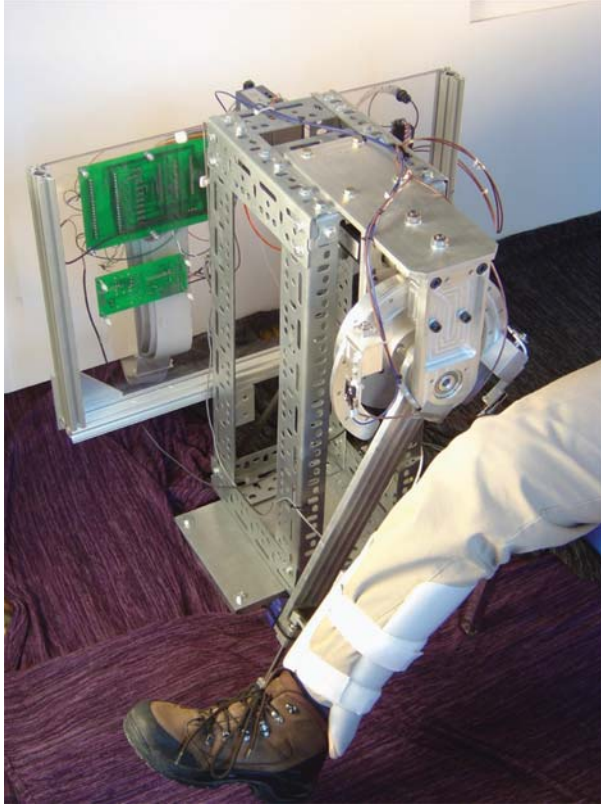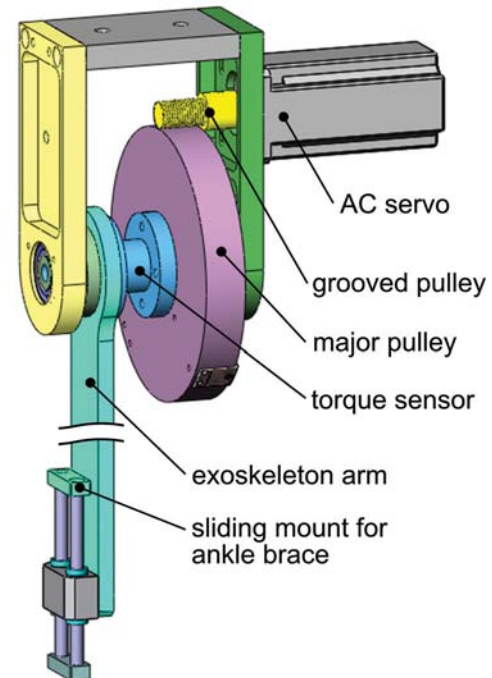
Fig. 1. 1-DOF exoskeleton coupled to a subject's leg.

Fig. 2. Diagram of the 1-DOF exoskeleton's motor, drive and arm assembly.

of leg-swing movements in the context of a computer-based pursuit task. Subjects moved their leg under three different experimental conditions: (1) leg unaided; (2) wearing the exoskeleton in 'baseline' state; and (3) wearing the exoskeleton with inertia compensation on. The effects of the exoskeleton on the frequency of leg swing are analyzed and discussed.

3. Exoskeleton design and construction

We designed and built a stationary 1-DOF exoskeleton for assisting knee flexion and extension exercises (Figure 1). Our aim was to use the pendular motion of the leg's shank as a scaled-down model of the swing motion of the entire leg when walking, and to investigate the effects of an active exoskeleton dynamics on the kinematics and energetics of leg-swing motion.

In order to specify the torque requirements for our 1-DOF exoskeleton, we surveyed reported values of knee torque during normal walking. Kerrigan et al. (2000) reported an extensive study on the knee joint torques of barefoot walking. The peak knee torques reported there were 0.34±0.15 (N m)/(kg m) for women and 0.32±0.15 (N m)/(kg m) for men. Thus for a male subject with body mass of 80 kg and height of 1.80 m, the peak knee torque during normal walking should be about 45 N m. DeVita and Hortobagyi (2003) reported peak knee torques ranging from 0.39 (N m)/kg for obese subjects to 0.97 (N m)/kg for lean

subjects. From these data, we concluded that an actuator–transmission combination capable of delivering about 20 N m of continuous torque would be sufficient to produce significantly large assistive torques.

Figure 2 shows a computer-aided design model of the exoskeleton's main assembly, consisting of a servo motor, a cable-drive transmission and a pivoting arm. The motor is a Kollmorgen (Radford, VA, USA) brushless direct-drive AC motor with a power rating of 0.99 kW and a continuous torque rating of 2.0 N m. The motor features a proprietary emulated encoder with a resolution of 65,536 counts. The transmission ratio of the exoskeleton's cable drive is 10:1, thus allowing a continuous torque output of 20.0 N m. The exoskeleton arm, fabricated in aluminum, has been made as lightweight as possible in order to reduce its inertial effects. The angular acceleration of the exoskeleton arm is measured by means of an MT9 digital inertial measurement unit from Xsens Technologies (Enschede, the Netherlands), operating at a sampling rate of 200 Hz. The unit features a three-axis linear accelerometer, and is mounted in such a way that two of the axes lie on the plane of rotation of the exoskeleton's arm (Figure 3). Angular acceleration is computed from the readings generated by those two axes.

The cable-drive solution was chosen in order to avoid problems associated with transmission backlash. Implementing admittance control in a system with a geared transmission can give rise to limit cycles due to backlash, particularly when damping compensation is applied (Aguirre-Ollinger et al., 2007b). A detail of the exoskeleton's drive system is shown in Figure 4. The torque sensor is located

Fig. 3. Mounting of the inertial measurement unit on the exoskeleton's arm.
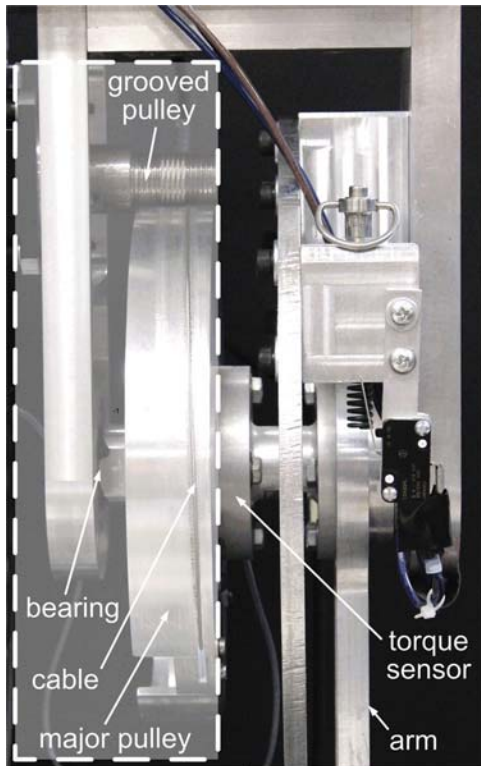

Fig. 4. Detail of the exoskeleton mechanism. The shaded rectangle contains the drive system components: grooved pulley (connected to the servo motor shaft), cable, major pulley and one bearing.

downstream from the cable drive, enabling the controller to mask any friction occurring on the cable and the motor.
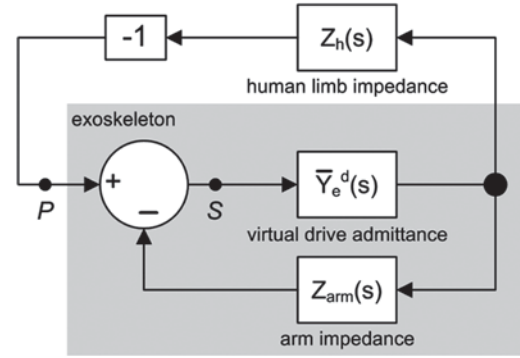

Fig. 5. Exoskeleton–human interaction model.

The tension of the cable is adjusted by means of a pair of adjustable plugs mounted on the inside of the major pulley.

For actual use the exoskeleton assembly is mounted on a rigid support frame (Figure 1). A custom-built ankle brace (Figure 3) couples the user's leg to the exoskeleton arm. The ankle brace is mounted on a sliding bracket in order to accommodate any possible radial displacement of the ankle relative to the device's center of rotation.

4. Assist through admittance control

In this section we discuss our general concept of exoskeleton-based assistance using admittance control. Then we examine the question of whether an admittance controller can be used to compensate for the inertia of the user's limb. A very simplified model of an admittance controller shows that, even assuming the very favorable case of rigid coupling between the user's limb and the exoskeleton, the coupled system will become unstable before any inertia compensation is accomplished. However, an approximate form of inertia compensation can be achieved by adding low-pass filtered acceleration feedback to the admittance controller.

Figure 5 shows a simplified model of the coupled system formed by the exoskeleton and the user's limb. Ideally, the admittance controller makes the exoskeleton drive (Figure 4) behave according to a virtual admittance model consisting of inertia moment $\bar{I}_e^d$, damping coefficient $\bar{b}_e^d$ and stiffness coefficient $\bar{k}_e^d$:

$$\bar{Y}_e^d(s) = \frac{s}{\bar{I}_e^d s^2 + \bar{b}_e^d s + \bar{k}_e^d}. \tag{1}$$

It can be seen in Figure 5 that the port of interaction between the user and the exoskeleton, P, is different from the torque sensor port S. In the physical exoskeleton, P corresponds to the ankle brace. Due to the impedance of the exoskeleton arm, these two ports have different admittances. The impedance of the exoskeleton's arm is given by

$$Z_{arm}(s) = \frac{I_{arm}s^2 + b_{arm}s + k_{arm}}{s}. \tag{2}$$

The most basic use of the admittance controller is to mask the dynamics of the exoskeleton arm from the user.

For example, if we include gravitational effects in the term k_{arm}, the weight of the exoskeleton's arm can be balanced by making $\bar{k}_e^d = -k_{\text{arm}}$. Likewise we can cancel the damping felt by the user by making $\bar{b}_e^d = -b_{\text{arm}}$.

One attractive feature of the admittance controller is that it can transition seamlessly from masking the impedance of the exoskeleton to actually assisting the user. For example, negative damping can be rendered at the interaction port in order to transfer energy to the user's limb. We have previously reported experiments (Aguirre-Ollinger et al., 2007a,b) in which negative damping was used to assist leg motion. Although negative damping made the isolated exoskeleton unstable, the subjects did remarkably well at maintaining control of their leg movements when using the exoskeleton. Those experiments relied in part on the passive damping of the human limb to insure the stability of the coupled system.

Our goal here is to make the exoskeleton increase the natural frequency of the leg, which can in theory be accomplished by compensating for the inertia of the leg. A possible strategy would be to generate a negative drive inertia $\bar{I}_e^d$, and use the inertia of the human limb I_h to guarantee the stability of the coupled system. However, as we will show, non-collocation of the exoskeleton's actuator and the torque sensor will cause the coupled system to become unstable even for *positive* values of $\bar{I}_e^d$, if these are too low in magnitude.

## 5. Inertia compensation and sensor non-collocation

The effects of the torque sensor's non-collocation can be demonstrated with a simplified model of the exoskeleton's mechanism and the human limb, as shown in Figure 6. The drive portion of the exoskeleton's model consists of the servo motor's inertia I_m (reflected on the output shaft) and an output inertia I_s, which comprises the mechanical components located between the cable and the torque sensor, i.e. the major pulley and the torque sensor's housing. The inertias are coupled by a spring of stiffness k_c representing the cable, and a damper b_c representing dissipative effects. The exoskeleton's arm inertia I_{arm} is rigidly coupled to I_s by the torque sensor at port S; we also assume a rigid coupling between the arm's inertia and the inertia of the human limb, I_h. The external torques acting on the system are the net human muscle torque τ_h and the exoskeleton's actuator torque τ_m. The torque measured by the sensor is τ_s. The exoskeleton's drive outputs are the angular velocity of the servo motor reflected on the output shaft, $w_m = \dot{\theta}_m$, and the output shaft's own angular velocity $w_s = \dot{\theta}_s$.

The relationship between the input torques and the output velocities of the exoskeleton can be expressed in terms of a two-port admittance in the Laplace domain, $\mathbf{Y}_e(s)$:

$$\begin{bmatrix} w_s(s) \\ w_m(s) \end{bmatrix} = \mathbf{Y}_e(s) \begin{bmatrix} \tau_s(s) \\ \tau_m(s) \end{bmatrix} = \begin{bmatrix} Y_e^{11} & Y_e^{12} \\ Y_e^{21} & Y_e^{22} \end{bmatrix} \begin{bmatrix} \tau_s \\ \tau_m \end{bmatrix}. \tag{3}$$
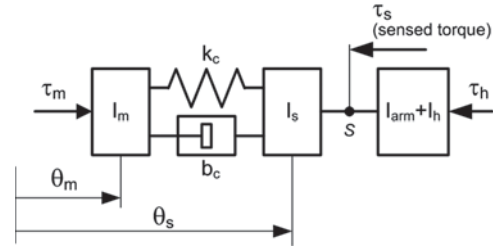
Fig. 6. Simplified model of the exoskeleton drive mechanism with inertial load. The servo motor and the torque sensor are non-collocated.
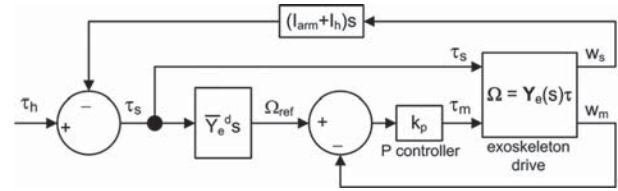
Fig. 7. Minimal admittance controller for the exoskeleton: an admittance model block is followed by a proportional velocity-tracking control.

We will employ a minimal admittance controller for the present analysis. The controller, shown in Figure 7 has two components:

- an admittance model $\bar{Y}_e^d(s)$ representing the desired admittance of the drive mechanism – in this case the desired dynamics are those of a pure inertia:

$$\bar{Y}_e^d = \frac{1}{\bar{I}_e^d s}; \tag{4}$$

- a proportional control law for velocity tracking:

$$\tau_m = k_p(w_{\text{ref}} - w_m) = k_p(\bar{Y}_e^d \tau_s - w_m). \tag{5}$$

From (3) and (5) we can derive the following expression for the exoskeleton's drive admittance under closed-loop control:

$$Y_e^s(s) = \frac{w_s(s)}{\tau_s(s)} = Y_e^{11}(s) + \frac{k_p Y_e^{12}(s)\left(\bar{Y}_e^d(s) - Y_e^{21}(s)\right)}{1 + k_p Y_e^{22}(s)}. \tag{6}$$

The inertial load acting on the exoskeleton drive is given by

$$Z_L(s) = (I_{\text{arm}} + I_h) s. \tag{7}$$

Thus the admittance presented to the muscle torque τ_h (Figure 6) is equal to the admittance of the coupled system formed by the closed-loop drive admittance $Y_e^s(s)$ and the load $Z_L(s)$. We now want to find the range of values of $\bar{I}_e^d$ for which the coupled system remains stable. This can be accomplished by applying the Nyquist stability criterion to

the open-loop transfer function of the coupled system, given by

$$G(s) = Z_L(s) Y_e^s(s)$$
$$= \frac{I_{\text{arm}} + I_h}{I_s} \frac{s^3 + \frac{k_p}{I_m}s^2 + \frac{k_c}{I_m}s + \frac{k_p k_c}{\bar{I}_e^d I_m}}{s^3 + \frac{k_p}{I_m}s^2 + \frac{k_c(I_m+I_s)}{I_m I_s}s + \frac{k_p k_c}{I_m I_s}}. \quad (8)$$

For simplicity we have neglected the damping of the exoskeleton's drive, i.e. made $b_c = 0$. The stability analysis for the non-collocated system, presented in Appendix A, yields the following condition for stability:

$$\bar{I}_e^d \geq \frac{I_m(I_{\text{arm}} + I_h)}{I_s + I_{\text{arm}} + I_h}. \quad (9)$$

If we consider $I_{\text{arm}} + I_h \gg I_s$, condition (9) can be reduced to

$$\bar{I}_e^d \geq I_m. \quad (10)$$

Thus if the virtual inertia $\bar{I}_e^d$ is set to less than the reflected inertia of the motor the coupled system will become unstable. Because the virtual inertia $\bar{I}_e^d$ cannot be negative, the admittance controller as it stands cannot compensate for the inertias of the exoskeleton arm or the human limb. In this situation, the net impedance opposing the action of the leg muscles will include inertia added by the exoskeleton arm. This is clearly undesirable because the arm's inertia will reduce the natural frequency of the human limb, which is the exact opposite of our strategy for assist. Therefore, in order to increase the agility of the user's movements, we need to devise a complementary control method that serves the double purpose of masking the inertia of the exoskeleton's arm and the inertia of the human limb itself.[1]
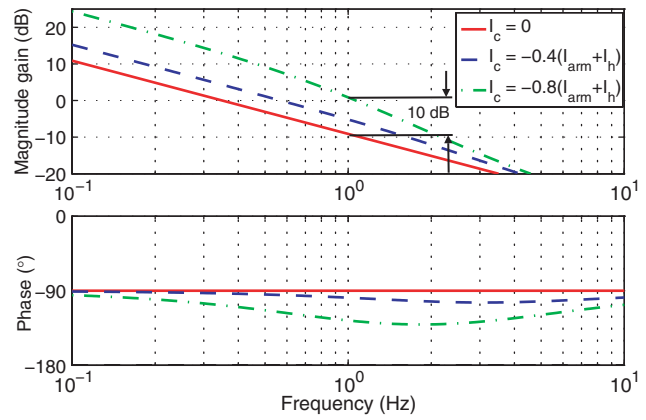
6. Emulated inertia compensation

We propose using an approximate form of inertia compensation that uses positive feedback of angular acceleration. A key observation is that typical voluntary movements of the knee joint occur at frequencies of less than 2 Hz. Therefore, for the purpose of assisting human motion, it is sufficient to provide acceleration feedback that is low-pass filtered at a cutoff frequency close to the maximum frequency of leg motion. Obviously this will not cause an exact cancellation of the human limb's inertia, but it can produce some of its desirable effects, particularly the increase in the pendulum frequency of the leg. Thus we refer to this effect as *emulated inertia compensation*.

Figure 8 shows the minimal admittance controller with the addition of emulated inertia compensation. The angular acceleration of the drive's output shaft is low-pass filtered at a cutoff frequency ω_{lo} and multiplied by a *negative* gain I_c. The transfer function of the emulated inertia compensator is given by

$$H_i(s) = \frac{I_c \omega_{lo} s}{s + \omega_{lo}}. \quad (11)$$
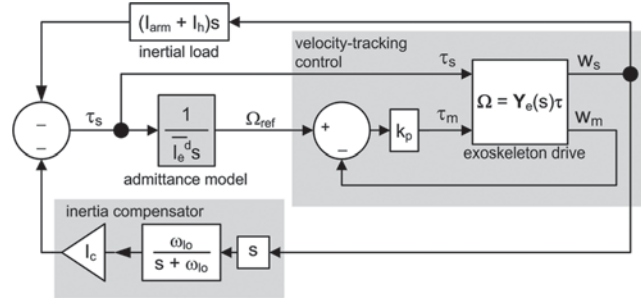
Fig. 8. Minimum admittance controller enhanced with emulated inertia compensation. The load inertia $I_{\text{arm}} + I_h$ represents the combined inertias of the exoskeleton arm and the human limb.

Fig. 9. Frequency–response plots of the closed-loop admittance $Y_e^h(s)$ of the coupled system formed by the exoskeleton drive with inertia compensation and the load inertia.

The load acting on the exoskeleton drive is again formed by the combined inertias of the exoskeleton arm (I_{arm}) and the human limb (I_h). Therefore, the open-loop transfer function of this new coupled system is given by

$$G_i(s) = [H_i(s) + Z_L(s)] Y_e^s(s). \quad (12)$$

The task is now to find the range of values of inertia compensation gain I_c that guarantees stability of the coupled system featuring emulated inertia compensation. The stability analysis for this system, presented in Appendix B, yields the following condition for stability:

$$I_c \geq -(I_h + I_{\text{arm}} + I_m). \quad (13)$$

Thus if we consider I_c as an inertia term at low frequencies, (13) suggests that a negative value of I_c can be used to compensate for the inertia of the load acting on the exoskeleton drive, which includes the inertia of the human limb, without losing stability.[2]

In order to get a sense of the controller's capability for compensating inertia, we examine the frequency response of the coupled system. We denote by $Y_e^h(s)$ the admittance

presented to the muscles' torque τ_h when the human limb's inertia I_h is coupled to the exoskeleton:

$$Y_e^h(s) = \frac{w_s(s)}{\tau_h(s)} = \frac{Y_e^s(s)}{1 + [H_i(s) + Z_L(s)]Y_e^s(s)}. \quad (14)$$

Figure 9 shows exemplary frequency–response plots of $Y_e^h(s)$ for different values of I_c. At low frequencies (i.e. frequencies in the range of human motion), the inertia compensator clearly increases the admittance of the system. As the frequency increases, all admittances converge to the value corresponding to $I_c = 0$. Figure 9 shows that for $I_c = -0.8(I_{\text{arm}} + I_h)$ the increase in admittance is about 10 dB at 1 Hz, which corresponds to a virtual reduction in load inertia of about 68%. With the values of I_{arm} and I_h employed, the virtual inertia opposing the muscles will be about $0.54 I_h$. In other words, wearing the exoskeleton at that value of I_c should feel similar to reducing the leg segment's inertia by about half.

Clearly, the model in Figure 8 is a considerable simplification of the physical exoskeleton, but it shows that the proposed control approach has the potential not only to compensate for the inertia of the exoskeleton's arm, but the inertia of the user's limb as well.

7. Admittance controller and emulated inertia compensator of the 1-DOF exoskeleton

7.1. Detailed implementation of the admittance controller

The controller implemented for the physical 1-DOF exoskeleton is shown in Figure 10. Its major components are an admittance controller and a feedback loop forming the inertia compensator. The admittance controller consists of an admittance model followed by a trajectory-tracking linear-quadratic (LQ) controller with an error-integral term (Stengel, 1994). The admittance model in (1) was converted to the following state space model:

$$\begin{bmatrix} \dot{\theta} \\ \ddot{\theta} \\ \dot{\xi} \end{bmatrix} = \begin{bmatrix} 0 & 1 & 0 \\ -\frac{\bar{k}_e^d}{\bar{I}_e^d} & -\frac{\bar{b}_e^d}{\bar{I}_e^d} & 0 \\ 1 & 0 & 0 \end{bmatrix} \begin{bmatrix} \theta \\ \dot{\theta} \\ \xi \end{bmatrix} + \begin{bmatrix} 0 \\ \frac{1}{\bar{I}_e^d} \\ 0 \end{bmatrix} \tau_{\text{net}}, \quad (15)$$

where θ is the angular position of the exoskeleton arm and $\xi = \int \theta \, dt$. The integral term ξ is employed to minimize tracking error. The input to the admittance model, τ_{net}, is the sum of the torque measured by the torque sensor, τ_s, plus the feedback torque from the inertia compensator. The above system can be expressed in compact form as

$$\dot{\mathbf{q}} = \bar{\mathbf{F}}_e^d q + \bar{\mathbf{G}}_e^d \tau_{\text{net}} \quad (16)$$

where $\mathbf{q}$ represents the state-space vector

$$\mathbf{q} = [\, \theta \quad \dot{\theta} \quad \xi \,]^T. \quad (17)$$

The admittance model uses numerical integration to generate the reference state trajectory $\mathbf{q}_{\text{ref}}(t)$ that will be tracked by the closed-loop LQ controller. Kinematic feedback consists of the servo motor's angle θ_m, measured by the emulated encoder. A state observer with a Kalman filter $\mathbf{C}(s)$ computes an estimate of the full feedback state. The controller was implemented in the QNX real-time operating system, using a sampling rate of 1 kHz.

The frequency response of the exoskeleton mechanism showed that the second-order linear time-invariant (LTI) model was sufficiently accurate for frequencies up to 10 Hz (Aguirre-Ollinger, 2009). The trajectory-tracking fidelity was estimated with the coefficient of determination, R^2. For a 2 Hz sinusoid the tracking fidelity was found to be 99.3%. Thus the admittance controller can accurately track angular trajectories in the typical frequency range of lower-limb motions.

7.2. Emulated inertia compensator

The estimated angular acceleration is low-pass filtered by means of a fourth-order Butterworth filter. In order to produce the inertia compensation effect, a negative feedback gain I_c is applied. This gain can be considered as a negative inertia term at low frequencies. This frequency was chosen after running a series of pilot tests on a few subjects, using different filter models and cutoff frequencies. At higher cutoff frequencies, the higher-frequency content in the acceleration feedback made it harder to control voluntary leg movements. Very low cutoff frequencies, on the other hand, reduced the fidelity of the inertia compensation effect due to the phase lag introduced by the filter. Thus the selected cutoff frequency represents a compromise between frequency content and phase lag.

For the upcoming analysis the admittance model is used only for masking the damping and weight of the exoskeleton. Assistance to the user comes exclusively from emulated inertia compensation. Given the location of the torque sensor (port S in Figure 10), the inertia felt by the user when $I_c = 0$ is the sum of the physical inertia of the exoskeleton's arm, I_{arm}, plus the virtual inertia of the exoskeleton's drive, $\bar{I}_e^d$. So in theory the inertia compensator has to counteract a total inertia $\bar{I}_e^d + I_{\text{arm}}$ before it can compensate for the inertia of the human leg.

7.3. Coupled stability conditions for interaction with the human limb

A stability analysis using the exoskeleton model of Figure 10 shows there is a range of negative values of I_c that can in theory produce a virtual reduction of the inertia of the human limb without loss of stability. The closed-loop admittance of the exoskeleton at the interaction port P is defined as

$$Y_e^p(s) = \frac{w_s(s)}{\tau_p(s)} \quad (18)$$
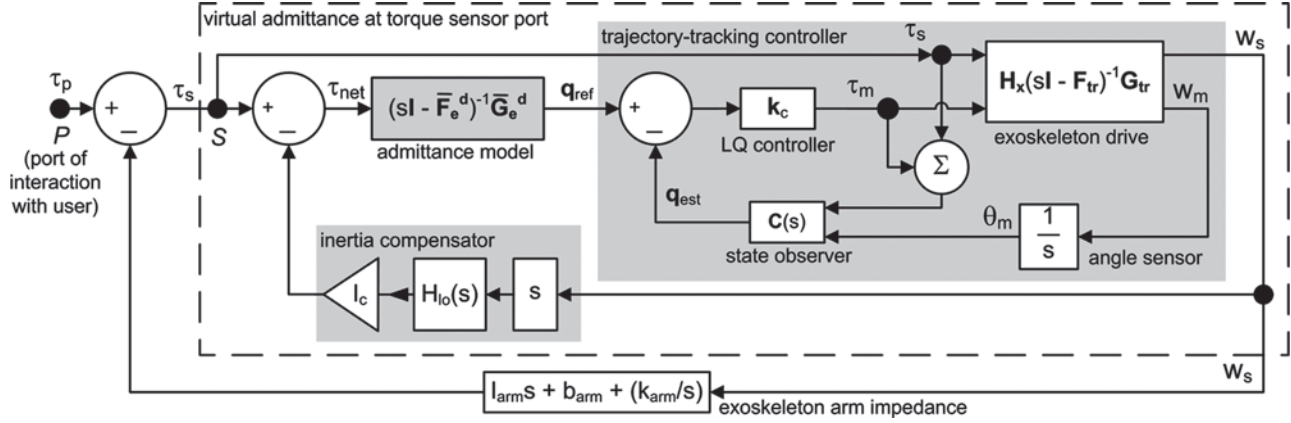
Fig. 10. Detailed model of the exoskeleton controller. A virtual admittance model generates a reference state trajectory $\mathbf{q}_{ref}$. The input to the admittance model is the sum of the torque sensor measurement τ_s plus the feedback torque from the inertia compensator. The reference trajectory $\mathbf{q}_{ref}$ is tracked by a closed-loop controller that uses an LQ regulator. The exoskeleton drive outputs are the angular velocity w_m of the servo motor reflected on the output shaft, and the output shaft's own angular velocity w_s. Servo motor's angle θ_m is measured by a proprietary feedback device that emulates an encoder. A state observer with a Kalman filter is employed to compute a full state estimate for feedback. In the inertia compensator, the angular acceleration feedback signal is low-pass filtered by a fourth-order Butterworth filter ($H_{lo}(s)$) with a cutoff frequency of 4 Hz. A negative feedback gain I_c emulates a negative inertia term at low frequencies.

where $\tau_p(s)$ is the torque exerted by the leg on the exoskeleton arm. The human leg segment is modeled as a second-order linear impedance:

$$Z_h(s) = \frac{I_h s^2 + b_h s + k_h}{s}. \tag{19}$$

The stability of the coupled system model can be determined from the frequency–response plot of the open-loop transfer function $\left[Y_e^p(s) Z_h(s)\right]^{-1}$. We computed the transfer function for $Y_e^p(s)$ using the identified parameters of the physical exoskeleton: $I_m = 0.0059$ kg m², $I_s = 0.0091$ kg m², $I_{arm} = 0.185$ kg m², $\omega_{n,e} = 1131$ rad/s and $\omega_{lo} = 25.1$ rad/s (4 Hz). The parameters assigned to the human limb model were $I_h = 0.26$ kg m², $b_h = 2.0$ (N m s)/rad and $k_h = 11.0$ (N m)/rad. The desired effect of coupling the exoskeleton to the human leg can be represented as multiplying the inertia of the leg segment I_h by a factor α_i such that $0 < \alpha_i < 1$. Treating I_c as an inertia term, the value of I_c that corresponds to a particular value of α_i is computed as

$$I_c = (\alpha_i - 1) I_h - I_{arm}. \tag{20}$$

Figure 11 shows frequency–response plots for the open-loop transfer function $\left[Y_e^p(s) Z_h(s)\right]^{-1}$ for three different values of α_i. The threshold for instability is approximately $\alpha_i = 0.53$, which means that almost half of the inertia of the leg segment could in theory be compensated before instability occurs.

Our approach to lower-limb assist can be viewed as shaping the admittance function that relates net muscle torque to the angular velocity of the leg segment. The admittance
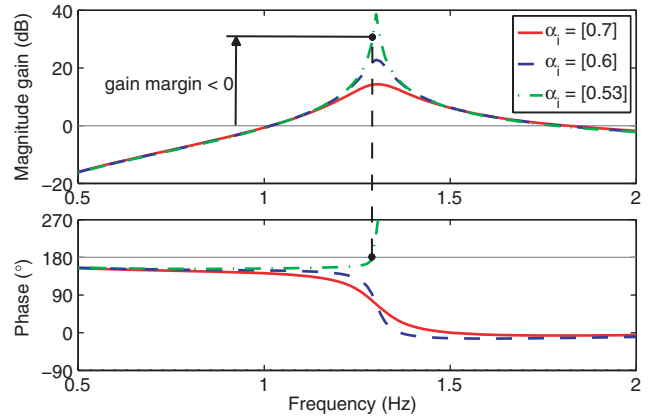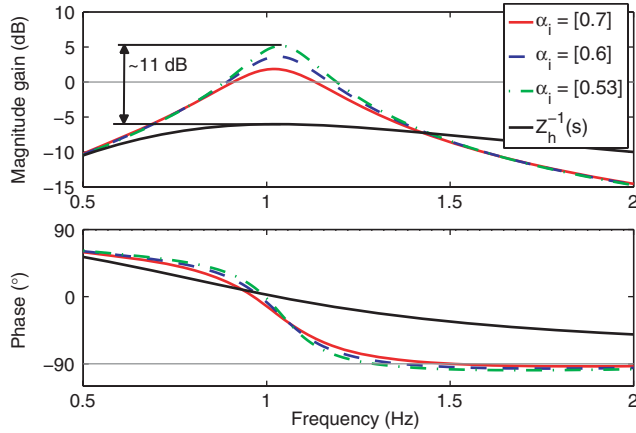

Fig. 11. Frequency–response plots of the open-loop transfer function $\left[Y_e^p(s) Z_h(s)\right]^{-1}$ of the coupled human limb-exoskeleton system for three different compensation factors α_i. Instability occurs at $\alpha_i = 0.53$.

presented to the muscles when the leg is coupled to the exoskeleton is given by

$$Y_e^h(s) = \frac{w_s(s)}{\tau_h(s)} = \frac{Y_e^p(s)}{1 + Z_h Y_e^p(s)}. \tag{21}$$

Emulated inertia compensation produces a virtual increase in the magnitude of the human leg's admittance over the typical frequency range of leg motion. Figure 12 shows frequency–response plots of the closed-loop admittance $Y_e^h(s)$ for the same values of α_i used before. In order to provide a comparison, the frequency response of the uncoupled leg's admittance Z_h^{-1} is plotted as well. It can be seen that the coupled leg-exoskeleton system displays

Fig. 12. Frequency–response plots of the admittance $Y_e^h(s)$ of the human limb coupled to the exoskeleton. Three different inertia compensation factors α_i are shown. For comparison purposes, the uncoupled leg's admittance Z_h^{-1} is also shown.

Fig. 13. Graphic user interface for the experimental task. The linear speed $\dot{x}_h$ of the subject's cursor is directly proportional to the leg's RMS angular velocity Ω_h. The linear speed $\dot{x}_{\text{ref}}$ of the subject's cursor is directly proportional to Ω_{ref}.

higher magnitudes of admittance over a frequency range of about 0.5 to 1.4 Hz (which can be considered typical for lower-limb movements), with the magnitude of the admittance peaking at about 1 Hz.

The virtual increase in the leg's admittance is only possible because emulated inertia compensation makes the exoskeleton's port admittance $Y_e^p(s)$ non-passive. The implication is that the exoskeleton is unstable in isolation, but can in theory be stabilized by the passive dynamics of the human limb. The stability of the coupled system and the exoskeleton's effect on the frequency of leg movements are verified experimentally in the next section.

8. Experiments with inertia compensation

We conducted an experiment to compare between free leg-swing motion, and leg-swing motion using the 1-DOF exoskeleton. The primary objective of the experiment was to determine how the subjects' selected frequency changed when wearing the exoskeleton. This effect can provide insights about how wearing an autonomous exoskeleton could alter the forward speed of walking. Changes produced by the stationary exoskeleton on the frequency of leg swing may have their correspondence in changes to step frequency when wearing an autonomous exoskeleton.

Assuming the angular trajectory of the swing motion to be approximately sinusoidal, the leg's average angular speed depends on both the amplitude and the frequency of the leg's movement. Although the primary design goal for the exoskeleton controller was to modulate swing frequency, the exoskeleton can modify swing amplitude as well.[3] Thus the experiment was designed with the idea of allowing the exoskeleton to influence both variables.

Keeping the sinusoidal motion assumption, the root mean square (RMS) angular velocity of leg swing is given by

$$\Omega_h = \sqrt{2}\pi A_c f_c \tag{22}$$
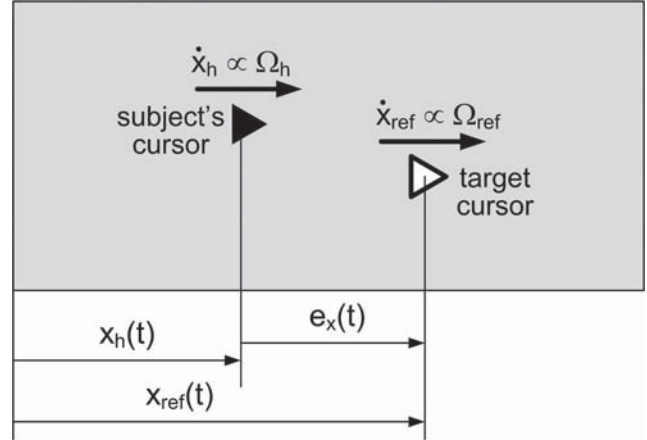
where A_c is the amplitude of leg swing in radians and f_c is the swing frequency in hertz. The experimental task gives the subjects a target value of RMS angular velocity, Ω_{ref}, to be matched or exceeded by swinging the leg. The task has the form of a race against a virtual target; it is presented to the user by means of a computer graphic interface shown schematically in Figure 13. The display shows two cursors that traverse the screen from left to right. The subject's cursor moves in response to the swing motion of the subject's leg; its linear speed is directly proportional to the leg's RMS angular velocity Ω_h. The 'target' cursor travels at a constant linear speed proportional to Ω_{ref}. For the actual experiment the leg's RMS angular velocity is computed in real time as a running average:

$$\Omega_h(t) = \sqrt{\frac{1}{T}\int_{t-T}^{t} \dot{\theta}(\tau)^2 \, d\tau}. \tag{23}$$

The time interval used is $T = 0.15$ s. The horizontal positions of the target cursor and the subject's cursor are given, respectively, by

$$x_{\text{ref}}(t) = \int_0^t \Omega_{\text{ref}} d\tau,$$

$$x_h(t) = \int_0^t \Omega_h(\tau) \, d\tau. \tag{24}$$

The position error of the subject's cursor relative to the target cursor is $e_x(t) = x_{\text{ref}}(t) - x_h(t)$.

The experiment consisted of a series of races between the subject's cursor and the target cursor. The standard duration of a trial was 15 s. The instruction to the subjects was to swing their leg fast enough to make their cursor pass the target cursor before the end of the trial. For all trials, the velocity of the target cursor, Ω_{ref}, was set to be 20% larger than the subject's preferred velocity of unassisted leg swing.
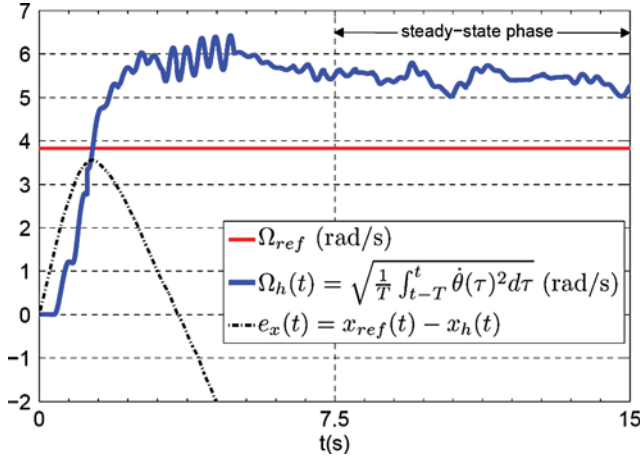
Fig. 14. Time trajectory of a race trial in the ASSIST condition. The plot shows the evolution of the subject's RMS angular velocity of leg swing, Ω_h, when tracking the reference value Ω_{ref}. Also shown is the corresponding time trajectory of the subject cursor's position error $e_x(t)$.

The time trajectory of a typical race trial with emulated inertia compensation is shown in Figure 14. Ω_h varies over the trial as indicated by (23). Eventually the action of the exoskeleton enables the subject to settle on a relatively uniform value of Ω_h that is larger than Ω_{ref}. The linear position error between cursors, $e_x(t)$, goes from positive to negative over the course of the trial, indicating that the subject's cursor has passed the target cursor. For the purposes of the present analysis we consider the last 7.5 s of the trial to be the 'steady-state' phase, i.e. the phase in which variations of Ω_h are at a minimum. By extension, the variations in swing frequency f_c and swing amplitude A_c are also at a minimum during this phase.

The rationale behind this task is that it places a lower bound on the subjects' RMS angular velocity, thus making the exercise somewhat demanding. Subjects are implicitly given freedom to select any combination of frequency and amplitude of leg swing in order to produce Ω_h. The assumption is that, when the exoskeleton is used, its dynamics will lead the subject to adopt a combination of frequency and amplitude that minimizes effort. The present analysis will focus exclusively on swing frequency when Ω_h has reached a steady-state value. A more comprehensive analysis of the exoskeleton's effect on the kinematics of leg swing will be presented in a future report.

Ten male healthy subjects participated in this study (body mass = 72.4±11.7 kg (mean ± SD); height = 178±6 cm; age = 22.1±2.9 years). None of the subjects had previous experience using the exoskeleton. The experimental protocol was approved by the Institutional Review Board of Northwestern University; all subjects gave their informed consent previous to participating in the experiment.

The race task was performed under three different experimental conditions:

- UNCOUPLED. The subject swings the leg unaided. The inertial measurement unit is temporarily attached to the ankle in order to generate angular velocity data from the sensor's gyros.
- BASELINE. The subject wears the exoskeleton with no inertia compensation ($I_c = 0$), thus being subject to the full inertia of the exoskeleton's arm. However, the weight of the exoskeleton's arm and the friction and damping of the exoskeleton's drive are cancelled by the admittance controller.
- ASSIST. The subject wears the exoskeleton with a specific level of inertia compensation, defined by the gain value I_c.

The number of trials executed was five in each of the UNCOUPLED and BASELINE conditions, and 11 in the ASSIST condition. For every trial performed, the steady-state leg-swing frequency $f_{c,ss}$ was the average frequency over the interval from 7.5 to 15 s. The hypothesis for the race experiments was that (1) in the BASELINE trials the exoskeleton arm's inertia would reduce the steady-state frequency of leg swing in comparison with the UNCOUPLED trials, and (2) the steady-state frequency would increase again in the ASSIST condition due to the inertia compensation effect. The method for computing the swing frequency consisted of decomposing the angular position trajectory of the leg, $\theta(t)$, into a set of components called intrinsic mode functions (Huang et al., 1998), and applying the Hilbert transform to the lowest-frequency component.[4] The procedure is described in Aguirre-Ollinger (2009).

We performed repeated-measures analysis of variation (ANOVA) with experimental condition (UNCOUPLED, BASELINE or ASSIST) as the factor and steady-state leg-swing frequency as the output variable. We computed the steady-state leg-swing frequency as the average of consecutive trials per subject per experimental condition.[5] If the effect of the experimental condition was found to be significant ($p < 0.05$), we would then use Tukey honestly significant difference (HSD) tests to determine specific differences between the means.

9. Experimental results

The net exoskeleton inertia presented to the subjects in the BASELINE condition was 0.22 kg m[2], which is equal to the sum of the arm inertia I_{arm} (0.185 kg m[2]) plus the virtual inertia of the drive mechanism, $\bar{I}_e^d$ (set to 0.035 kg m[2] for this experiment). This being a first experiment, inertia compensation gains were applied conservatively. The value of I_c was selected through a series of calibration trials preceding the ASSIST trials. For each subject, the selected value of I_c was the one that caused a first noticeable reduction in ability to switch the direction of leg movement. The resulting range of values for I_c was -0.125±0.024 kg m[2] (mean±SD). Thus in a sense the net exoskeleton inertia of 0.22 kg m[2] was not fully compensated for in these experiments.
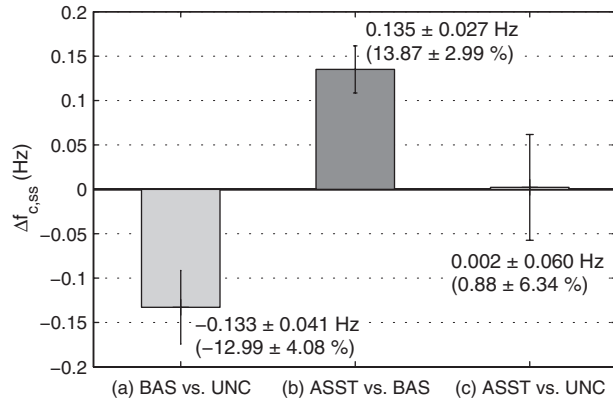
Fig. 15. Steady-state frequency of leg swing ($f_{c,ss}$). Bars show the mean change in steady-state frequency between experimental conditions: (a) BASELINE vs. UNCOUPLED, (b) ASSIST vs. BASELINE, (c) ASSIST vs. UNCOUPLED. Error bars are ± SEM. Also indicated is the mean change in steady-state frequency as a percentage of the subject's UNCOUPLED steady-state frequency.

The experimental conditions were found to have a significant effect on the steady-state leg-swing frequency (ANOVA: $p = 0.03$; HSD: BASELINE < UNCOUPLED, ASSIST > BASELINE). Figure 15 shows the mean change in steady-state frequency between experimental conditions. Error bars represent the standard error of the mean (SEM). Subjects performing the race task in the BASELINE condition showed a considerable reduction in swing frequency with respect to the UNCOUPLED case (−12.99±4.08%). This reduction is consistent with the exoskeleton arm's inertia reducing the natural frequency of the leg. The ASSIST condition in turn increased the steady-state frequency with respect to the BASELINE case (13.87±2.99%), suggesting that emulated inertia compensation effectively counteracts the arm's inertia. There was no significant difference between steady-state frequencies for the ASSIST and UNCOUPLED conditions (0.88±6.34%). Thus for practical purposes inertia compensation brought the natural frequency of the leg back to levels corresponding to those of the unassisted leg. Interestingly, this result was achieved with inertia compensation gains I_c that in theory were not large enough in magnitude to fully compensate for the inertia of the exoskeleton, let alone compensate for the inertia of the human limb.

It is instructive to examine the differences in the exoskeleton's measured impedance between the BASELINE and ASSIST conditions. We computed the impedance at the torque sensor port at the mean steady-state frequency of the leg swing. The impedance was obtained from the fast Fourier transforms of the measured torque, τ_s, and the measured angular velocity, w_m. The mean impedance value was $-0.257 + 1.031i$ (N m s)/rad for the BASELINE condition.[6] The mean impedance value for the ASSIST condition was $-0.667 + 0.450i$ (N m s)/rad. Thus the real part of the impedance becomes more negative when inertia compensation is present. In other words, the emulated inertia compensator, besides modulating the frequency of swing, also adds negative damping. As a consequence the exoskeleton in the ASSIST condition produces a net transfer of energy to the user's leg.

10. Discussion

We have developed a control method that, in a sense, goes against conventional thinking about human–robot interaction. Impedance and admittance control methods for human–robot interaction typically emphasize coupled stability. Robot passivity has been long established as a condition for guaranteed coupled stability between the robot and any passive environment (Colgate and Hogan, 1988, 1989). However, our strategy for lower-limb assist is based on making the exoskeleton produce a virtual increase in the leg's admittance. This can only be accomplished if the exoskeleton exhibits non-passive behavior, with the implication that the exoskeleton is unstable in isolation. Stable interaction between the exoskeleton and the lower extremities is possible due in part to the passive dynamics of the leg. However, the role of human sensorimotor control needs to be considered as well. Burdet et al. (2001) has reported that humans adapt well to unstable manual tasks when perturbation forces are normal to the direction of the intended motion. In the case of an active exoskeleton, destabilizing forces act on the direction of the desired motion. The human's mechanism for adapting to such forces is a potential area of research.

In the experiments reported here, user safety was given preeminence over performance. Thus the inertia compensation gains (I_c) were applied conservatively. We found that subjects consistently reduced the frequency of leg swing in the exoskeleton's BASELINE condition, but were able to recover their normal frequency of leg swing when inertia compensation was applied. Surprisingly, this effect was accomplished with inertia compensation gains that on average were 43% smaller than the theoretical value needed to fully compensate for the inertia of the exoskeleton. This larger-than-expected increase in frequency may be explained by an attendant increase in the level of co-contraction of the muscles controlling flexion and extension of the knee joint. A high level of co-contraction would increase the stiffness of the leg joint, thus making an additional contribution to raising the natural frequency of the limb segment. Using electromyography (EMG) measurements in future experiments may clarify whether an increase in co-contraction actually occurs.

While in general the swing frequencies achieved by the subjects in the ASSIST condition were not larger than in the UNCOUPLED case, we did not find anything to suggest that larger negative values of I_c cannot be employed in future experiments. The key is probably to run longer series of trials, giving the subjects more time to adapt to

the exoskeleton's dynamics. In a few separate trials we have had subjects interact comfortably with the exoskeleton at I_c gains as large as -0.24 kg m^2.

The implementation discussed here was restricted to single-joint control, but it can in principle be transferred to multi-joint control. Emulated inertia compensation is expected to have an effect on the swing phase of walking. Therefore, the design we envisage for a wearable exoskeleton is a hip-mounted device with actuators assisting leg motion on the sagittal plane. Hip abduction/adduction may be allowed by an unactuated degree of freedom of the mechanism. Such a design avoids placing distal masses on the leg, thereby reducing the handicap on agility associated with loading the leg (Browning et al., 2007; Royer and Martin, 2005).

The cable drive transmission performed remarkably well in producing an active admittance behavior without the issue of limit cycles. However, there is a limit to the transmission ratio that can be achieved by a cable drive, which in turn may require the use of a relatively large actuator in order to assist walking. However, this might offset the expected reduction in metabolic cost during leg swing. The mass added by the exoskeleton at the subject's center of mass (COM) can increase the metabolic cost of redirecting the COM at each step (Donelan et al., 2002). A highly geared transmission could allow the use of less massive motors, but at the cost of having to solve the limit-cycle issue in control rather than hardware.

11. Conclusions

Our approach to exoskeleton control is based on making the exoskeleton shape the dynamics of the human limb. This paper focused on one particular strategy for lower-limb assist: compensating for the inertia of the legs in order to increase their natural frequency. To achieve this effect, the controller has to first overcome the handicap introduced by the exoskeleton's own inertia, which tends to actually *reduce* the natural frequency of the legs.

Admittance control is a well-established method for masking the stiffness and the damping of a mechanical system (Newman, 1992). However, non-collocation of the torque sensor makes it unfeasible for the exoskeleton to follow an admittance model with a negative inertia term. Instead, we have emulated inertia compensation through positive feedback of the low-pass filtered angular acceleration. The effect resembles inertia compensation in that it produces a virtual increase in the magnitude of the human leg's admittance at typical frequencies of leg motion. Emulated inertia compensation makes the exoskeleton exhibit active admittance, and thus behave as a source of mechanical energy to the human limbs. Although active admittance makes the exoskeleton unstable in isolation, subjects in our experiment were able to adapt to the destabilizing effects of the exoskeleton, and increase their frequency of leg swing in the process. However, the effects of wearing the exoskeleton on muscle activation and metabolic consumption have yet to be studied.

The main application we envisage for our active-admittance control is assisting the swing phase of walking. For our future research we plan to develop a wearable exoskeleton to test the effects of inertia compensation on actual walking. Specific research objectives include determining how the exoskeleton affects the user's selected combination of step frequency and step length, and determining whether inertia compensation can enable walking at higher speeds with a metabolic cost lower than that corresponding to unassisted walking.

Notes

1. Note that the exoskeleton arm's inertia cannot be compensated for by placing the force or torque sensor at the port of interaction between the human limb and the exoskeleton arm (e.g. the ankle brace in Figure 3). All this will accomplish is changing the condition for coupled stability to

$$\bar{I}_e^d \geq \frac{I_m I_h}{I_s + I_{\text{arm}} + I_h}.$$

2. An alternative solution would be to make the inertia compensator part of the admittance model itself, i.e. define $\bar{Y}_e^d(s)$ as

$$\bar{Y}_e^d(s) = \frac{1}{\bar{I}_e^d s + H_i(s)}.$$

Because of the compliance of the exoskeleton's drive, this solution is not identical to adding $H_i(s)$ as a feedback loop. In this case the range of values of I_c that guarantee stability (assuming $\omega \ll \omega_{n,e}$) is given by

$$I_c \geq -I_m - \frac{k_p}{\omega_{lo}} \left(1 - \frac{I_s}{I_m + I_s + I_{\text{arm}} + I_h}\right).$$

This condition has the disadvantage of making k_p play a dual role: determining the performance of the trajectory control, and determining the stability of the coupled system. Therefore, it forces a compromise in the design of the controller. And unlike the solution placing $H_i(s)$ on a feedback loop, this solution does not allow to set I_c independently of ω_{lo}.

3. For example, when $I_c = 0$, the exoskeleton behaves as a pure inertia. If the leg is modeled as a second-order system, it is easy to see that the added inertia will not only cause a reduction in the natural frequency of the leg segment, but also a reduction in the damping ratio of the leg. The latter effect may result in an increase in leg-swing amplitude.

4. Although the steady-state frequency could be computed by other methods such as fast Fourier transform, the Hilbert transform provides information on time variations in the frequency of a signal, thus allowing us to detect transient behaviors of $\theta(t)$ over the time span of the signal.

5. The first trial in each experimental condition was dropped from the computation of the average. Any difficulties that the subject has adapting to a new experimental condition will show especially in the first trial. Therefore, this trial is

not considered to be representative of the subject's overall performance for that condition.

6. Although the exoskeleton in the BASELINE condition ($I_c = 0$) is theoretically passive at the interaction port P (see Figure 10), a negative value of virtual damping $\bar{b}_e^d$ is necessary to mask the physical damping of the arm. Hence the negative real part (-0.257 (N m s)/rad) of the measured impedance.

References

Aguirre-Ollinger G (2009) Active impedance control of a lower-limb assistive exoskeleton. Dissertation, Northwestern University, Evanston, IL.

Aguirre-Ollinger G, Colgate J, Peshkin M and Goswami A (2007a). A 1-DOF assistive exoskeleton with virtual negative damping: effects on the kinematic response of the lower limbs. In: *IEEE/RSJ International Conference on Intelligent Robots and Systems, 2007 (IROS 2007)*, 1938–1944, 29 October - 2 November, San Diego, CA, USA.

Aguirre-Ollinger G, Colgate J, Peshkin M and Goswami A (2007b). Active-impedance control of a lower-limb assistive exoskeleton. In: *IEEE 10th International Conference on Rehabilitation Robotics, 2007 (ICORR 2007)*, 188–195, 13–15 June, Noordwijk, The Netherlands.

Banala S, Agrawal SK, Fattah A, Krishnamoorthy V, Hsu W-L, Scholz J, et al. (2006) Gravity-balancing leg orthosis and its performance evaluation. *IEEE Transactions on Robotics* 22(6): 1228–1239.

Banala S, Kim S, Agrawal S and Scholz J (2009). Robot assisted gait training with active leg exoskeleton (ALEX). *IEEE Transactions on Neural Systems and Rehabilitation Engineering* 17(1): 2–8.

Browning RC, Modica JR, Kram R and Goswami A (2007) The effects of adding mass to the legs on the energetics and biomechanics of walking. *Medicine and Science in Sports and Exercise* 39(3): 515–525.

Buerger S and Hogan N (2007) Complementary stability and loop shaping for improved human-robot interaction. *IEEE Transactions on Robotics* 23(2): 232–244.

Burdet E, Osu R, Franklin D, Milner T and Kawato M (2001) The central nervous system stabilizes unstable dynamics by learning optimal impedance. *Nature* 414: 446–449.

Colgate E and Hogan N (1989) The interaction of robots with passive environments: Application to force feedback control. In: *Fourth International Conference on Advanced Robotics*. Berlin: Springer-Verlag.

Colgate J and Hogan N (1988) Robust control of dynamically interacting systems. *International Journal of Control* 48(1): 65–88.

DeVita P and Hortobagyi T (2003) Obesity is not associated with increased knee joint torque and power during level walking. *Journal of Biomechanics* 36: 1355–1362.

Doke J, Donelan JM and Kuo AD (2005) Mechanics and energetics of swinging the human leg. *Journal of Experimental Biology* 208: 439–445.

Dollar A and Herr H (2008) Lower extremity exoskeletons and active orthoses: Challenges and state of the art. *IEEE Transactions on Robotics* 24(1): 144–158.

Donelan J, Kram R and Kuo A (2002). Mechanical work for step-to-step transitions is a major determinant of the metabolic cost of human walking. *Journal of Experimental Biology* 205: 3717–3727.

Ferris D, Sawicki G and Daley M (2007) A physiologist's perspective on robotic exoskeletons for human locomotion. *International Journal of Humanoid Robotics* 4(3): 507–528.

Ferris D, Sawicki G and Domingo A (2005) Powered lower limb orthoses for gait rehabilitation. *Topics in Spinal Cord Injury Rehabilitation* 11(2): 34–49.

Huang N, Shen Z, Long S, Wu M, Shih H, Zheng Q, et al. (1998) The empirical mode decomposition and the Hilbert spectrum for nonlinear and non-stationary time series analysis. *Proceedings of the Royal Society London A* 454: 903–995.

Jezernik S, Colombo G and Morari M (2004) Automatic gait-pattern adaptation algorithms for rehabilitation with a 4-dof robotic orthosis. *IEEE Transactions on Robotics and Automation* 20(3): 574–582.

Kawamoto H and Sankai Y (2005) Power assist method based on phase sequence and muscle force condition for HAL. *Advanced Robotics* 19(7): 717–734.

Kazerooni H, Racine J-L, Huang L and Steger R (2005). On the control of the berkeley lower extremity exoskeleton (BLEEX). In: *Proceedings of the 2005 IEEE International Conference on Robotics and Automation, 2005 (ICRA 2005)*, 4353–4360, 18–22 April, Barcelona, Spain.

Kerrigan D, Riley P, Nieto TJ and Della Croce U (2000) Knee joint torques: A comparison between women and men during barefoot walking. *Archives of Physical Medicine and Rehabilitation* 81: 1162–1165.

Kuo AD (2001) A simple model of bipedal walking predicts the preferred speed–step length relationship. *Journal of Biomechanical Engineering* 123(3): 264–269.

Lee S and Sankai Y (2002) Power assist control for walking aid with HAL-3 based on EMG and impedance adjustment around knee joint. In: *EEE/RSJ International Conference on Intelligent Robots and Systems, 2002, I*, vol 2, 1499–1504, 30 September - 4 October, Lausanne, Switzerland.

Lee S and Sankai Y (2003) The natural frequency-based power assist control for lower body with HAL-3. In: *IEEE International Conference on Systems, Man and Cybernetics*, vol 2, 1642–1647, 5–8 October, Washington, DC, USA.

Lee S and Sankai Y (2005) Virtual impedance adjustment in unconstrained motion for an exoskeletal robot assisting the lower limb. *Advanced Robotics* 19(7): 773–795.

Newman W (1992) Stability and performance limits of interaction controllers. *Journal of Dynamic Systems, Measurement, and Control* 114(4): 563–570.

Royer TD and Martin PE (2005) Manipulations of leg mass and moment of inertia: Effects on energy cost of walking. *Medicine and Science in Sports and Exercise* 37(4): 649–656.

Sawicki G and Ferris D (2009) Powered ankle exoskeletons reveal the metabolic cost of plantar flexor mechanical work during walking with longer steps at constant step frequency. *Journal of Experimental Biology* 212: 21–31.

Stengel R (1994) *Optimal Control and Estimation*. New York, NY: Dover Publications, Inc.

Uemura M, Kanaoka K and Kawamura S (2006) Power assist systems based on resonance of passive elements. In: *2006 IEEE/RSJ International Conference on Intelligent Robots and Systems*, 4316–4321, 9–13 October, Beijing, China.

Veneman J, Kruidhof R, Hekman E, Ekkelenkamp R, Van Asseldonk E and van der Kooij H (2007) Design and evaluation of the lopes exoskeleton robot for interactive gait rehabilitation.

IEEE Transactions on Neural Systems and Rehabilitation Engineering 15(3): 379–386.

Walsh C, Paluska D, Pasch K, Grand W, Valiente A and Herr H (2006) Development of a lightweight, underactuated exoskeleton for load-carrying augmentation. In: *Proceedings 2006 IEEE International Conference on Robotics and Automation, 2006 (ICRA 2006)*, 3485–3491. 15–19 May, Orlando, FL, USA.

A. Stability of a simple con-collocated system under admittance control

We begin by testing $G(s)$ in (8) for right half-plane poles. The characteristic polynomial of $G(s)$ yields the following Routh array:

$$\left[1, \frac{k_p}{I_m}, \quad \frac{k_c(I_m + I_s)}{I_m I_s}, \quad \frac{k_p k_c}{I_m I_s}\right] \quad (25)$$

Because all the coefficients involved are positive, no changes of sign occur in the Routh array. In consequence, the open-loop transfer function $G(s)$ has no right half-plane poles. Therefore, a sufficient condition for the stability of the closed-loop system is that $G(s)$ produces no encirclements of -1. The task is therefore to find the range of values of $\bar{I}_e^d$ that simultaneously satisfy

$$\mathrm{Re}\{G(j\omega)\} > -1,$$
$$\mathrm{Im}\{G(j\omega)\} = 0. \quad (26)$$

$G(j\omega)$ is given by

$$G(j\omega) = \frac{a(\omega) + jb(\omega)}{c(\omega) + jd(\omega)} \quad (27)$$

where

$$a(\omega) = \bar{I}_e^d I_m (I_\mathrm{arm} + I_h)\omega^4 - k_c \bar{I}_e^d (I_\mathrm{arm} + I_h)\omega^2,$$
$$b(\omega) = -\bar{I}_e^d k_p (I_\mathrm{arm} + I_h)\omega^3 + k_p k_c (I_\mathrm{arm} + I_h)\omega,$$
$$c(\omega) = \bar{I}_e^d I_m I_s \omega^4 - \bar{I}_e^d k_c (I_m + I_s)\omega^2,$$
$$d(\omega) = -k_p I_s \bar{I}_e^d \omega^3 + k_p k_c \bar{I}_e^d \omega. \quad (28)$$

From (26) we can derive the following system of equations:

$$\frac{a(\omega)c(\omega) + b(\omega)d(\omega)}{c(\omega)^2 + d(\omega)^2} > -1,$$
$$\frac{b(\omega)c(\omega) - a(\omega)d(\omega)}{c(\omega)^2 + d(\omega)^2} = 0. \quad (29)$$

After solving (29) for $\bar{I}_e^d$ and ω we arrive at the following stability condition:

$$\bar{I}_e^d \geq \frac{I_m(I_\mathrm{arm} + I_h)}{I_s + I_\mathrm{arm} + I_h}. \quad (30)$$

B. Stability of a simple con-collocated system with emulated inertia compensation

We will restrict the analysis to the limit case $\bar{I}_e^d = I_m$. Substituting terms in (12) yields the following expression for the open-loop transfer function:

$$G_i(s) = K_i \frac{N_i(s)}{D_i(s)} \quad (31)$$

where

$$K_i = \frac{I_\mathrm{arm} + I_h}{I_s},$$

$$N_i(s) = s^4$$
$$+ \frac{k_p(I_h + I_\mathrm{arm}) + \omega_{lo} I_m (I_\mathrm{arm} + I_h + I_c)}{I_m(I_\mathrm{arm} + I_h)}s^3$$
$$+ \frac{\omega_{n,e}^2 I_m I_s(I_\mathrm{arm} + I_h) + \omega_{lo} k_p(I_m + I_s)(I_\mathrm{arm} + I_h + I_c)}{I_m(I_m + I_s)(I_\mathrm{arm} + I_h)}s^2$$
$$+ \frac{\omega_{n,e}^2 I_s(k_p(I_\mathrm{arm} + I_h) + \omega_{lo} I_m(I_\mathrm{arm} + I_h + I_c))}{I_m(I_m + I_s)(I_\mathrm{arm} + I_h)}s$$
$$+ \frac{\omega_{lo}\omega_{n,e}^2 k_p I_s(I_\mathrm{arm} + I_h + I_c)}{I_m(I_m + I_s)(I_\mathrm{arm} + I_h)},$$

$$D_i(s) = s^4 + \frac{k_p + \omega_{lo} I_m}{I_m}s^3 + \frac{\omega_{lo} k_p + \omega_{n,e}^2 I_m}{I_m}s^2$$
$$+ \frac{\omega_{n,e}^2(k_p + \omega_{lo}(I_m + I_s))}{I_m + I_s}s + \frac{\omega_{lo} k_p \omega_{n,e}^2}{I_m + I_s}. \quad (32)$$

In the above equations $\omega_{n,e}$ is the natural frequency of the exoskeleton drive, given by

$$\omega_{n,e} = \sqrt{\frac{k_c(I_m + I_s)}{I_m I_s}}. \quad (33)$$

The Routh array of $D_i(s)$ in (32) is

$$\left[1, \frac{\omega_{lo} I_m + k_p}{I_m}, \frac{k_p\omega_{lo} + \omega_{n,e}^2 I_m}{I_m}, \frac{\omega_{n,e}^2(k_p + \omega_{lo}(I_m + I_s))}{I_m + I_s}, \frac{\omega_{lo}\omega_{n,e}^2 k_p}{I_m + I_s}\right]. \quad (34)$$

Because no changes of sign occur in the Routh array, it follows that $G_i(s)$ has no right half-plane poles. Therefore, as in the previous analysis, a sufficient condition for stability is that the open-loop transfer function produces no encirclements of -1. The analysis can be simplified considerably by limiting it to the case $\omega \ll \omega_{n,e}$, which yields the following expression for $G_i(j\omega)$:

$$G_i(j\omega) = \frac{a_i(\omega) + jb_i(\omega)}{c_i(\omega) + jd_i(\omega)} \quad (35)$$

where

$$a_i(\omega) = -I_m I_s[I_\mathrm{arm}(k_p + \omega_{lo} I_m) + I_h k_p + \omega_{lo} I_m(I_h + I_c)]\omega^2,$$
$$b_i(\omega) = -I_m^2 I_s(I_\mathrm{arm} + I_h)\omega^3 + I_m I_s \omega_{lo} k_p(I_\mathrm{arm} + I_h + I_c)\omega,$$
$$c_i(\omega) = -I_m^2 I_s[k_p + \omega_{lo}(I_m + I_s)]\omega^2,$$
$$d_i(\omega) = -I_m^2 I_s(I_m + I_s)\omega^3 + \omega_{lo} k_p I_m^2 I_s \omega. \quad (36)$$

Solving for $\mathrm{Re}\{G_i(j\omega)\} > -1$ and $\mathrm{Im}\{G_i(j\omega)\} = 0$ yields the following condition:

$$I_c \geq -(I_h + I_\mathrm{arm} + I_m). \quad (37)$$